Molecules in intense laser fields: Enhanced ionization in a one-dimensional model of H_2

Hengtai Yu, Tao Zuo,* and André D. Bandrauk
Laboratoire de Chimie Théorique, Faculté des sciences, Université de Sherbrooke, Sherbrooke, Québec, Canada J1K 2R1
(Received 14 May 1996)

A one-dimensional model of H_2 is used to examine the nonlinear behavior of a pair of electrons in the presence of intense laser fields and fixed nuclei. We present ionization rates of H_2 at different frequencies and intensities of short intense electromagnetic pulses by solving exactly the time-dependent Schrödinger equation for the above system as a function of internuclear distance. Anomalously high ionization rates are found at large critical internuclear separations, akin to similar results found previously in the one-electron molecule H_2^+. Independent one-electron and simultaneous two-electron ionizations are identified from the numerical simulations to occur at different intensities and frequencies. Field-induced barrier suppression models are shown to explain qualitatively the numerical results. [S1050-2947(96)08310-2]

PACS number(s): 42.50.Hz, 32.80.Rm

I. INTRODUCTION

The behavior of molecules in intense static electric and magnetic fields was considered as early as 1961 by Hiskes [1] and subsequently by Hanson [2] in 1975. Current available intense laser sources allow one to reexamine the general problem of molecules in interaction with intense electromagnetic fields, well beyond the perturbative limit. Earlier experimental investigations of H_2 in intense laser fields have led to the discovery of the molecular analog of atomic above threshold ionization (ATI) [3–8], above threshold dissociation (ATD) [3–6,9], and laser-induced avoided crossings [5,6,10–12]. Recent experiments have led to the discovery of anomalous Coulomb explosions occurring at large internuclear distances in symmetric diatomics [13–15]. This can be explained from one-electron models of ionization of symmetric molecules by the phenomenon of charge resonance enhanced ionization (CREI) [16,17], which is a combination of static field barrier suppression [18–20] and dynamic localization of the electron by the laser field [16,17]. Thus for *odd* electron systems, the first electronic transition moment varies as $R/2$ [12,21], where R is the internuclear distance. This introduces a very large coupling at large R between the single unpaired electron and the external field, larger than the first transition energy. This creates instantaneously two dressed states of the system at the peak of the field intensity E_0 with energy separation eE_0R, the potential energy difference of the electron between the two nuclei in the presence of the external electromagnetic field [17]. The energy eE_0R is equivalently twice the Rabi frequency for the first electronic transition. This has been shown to limit the maximum number of molecular harmonics [16] generated in such odd-electron molecular systems and also determines the critical internuclear distances R_c where CREI occurs due to both dynamical localization and static field barrier suppression [19] . Complete electron-nuclear non-Born-Oppenheimer full dynamical calculations confirm CREI as the predominant mechanism in Coulomb explosions [22,23] .

The aim of the present work is to examine CREI in a one-dimensional (1D) model of H_2, or equivalently the nonlinear, nonperturbative behavior of a pair of electrons in the presence of an intense external electromagnetic pulse and the static Coulomb field of two nuclei fixed at R. Previous time-dependent 1D calculations for two-electron atomic (one-nucleus) systems [24,25] have provided insight into atomic one-electron versus two-electron photoionization processes. A previous 1D model of H_2 examined the high frequency behavior of this molecule in the space translation representation [26]. We have also shown previously that 3D linear H_3^{2+}, a one-electron system, will bind three protons in high intensity and high frequency fields [27]. In the present paper we examine a 1D model of H_2 for wavelengths of 1064 and 532 nm and intensities $10^{14} \leqslant I \leqslant 10^{15}$ cm/W^2 and various internuclear distances R. We find that enhanced ionization also occurs at large R for two-electron molecular systems, both in the one-electron sequential low intensity ($I \geqslant 10^{14}$ W/cm^2) ionization regime and in the simultaneous two-electron high intensity ($I \geqslant 10^{15}$ W/cm^2) ionization regime. Recent classical calculations show similar phenomena in multiphoton ionization of clusters [28,29]. Our calculations are therefore a quantum confirmation of enhanced multiphoton ionization of molecules at large internuclear distances.

II. NUMERICAL METHOD

Due to the large mass of the nuclei in the H_2 molecule, we restrict ourselves to the Born-Oppenheimer approximation. The two nuclei are treated as fixed, the positions of which are considered as parameters in the electronic Hamiltonian. The time-dependent Schrödinger equation (TDSE) for the H_2 molecule in one dimension has the form

$$i\frac{\partial}{\partial t}\Psi(x_1,x_2,t)=[H(x_1,x_2,t)+V_{\text{ext}}(x_1,x_2,t)]\Psi(x_1,x_2,t), \tag{1}$$

where the electronic Hamiltonian is

*Present address: Office of the Superintendent of Financial Institutions Canada, 255 Albert Street, Ottawa, Ontario, Canada K1A 0H2.

$$H(x_1,x_2,t)=H_k+V_c, \quad H_k=-\frac{1}{2}\left(\frac{\partial^2}{\partial^2 x_1}+\frac{\partial^2}{\partial^2 x_2}\right), \quad (2)$$

$$V_c=-\left[c+\left(x_1-\frac{R}{2}\right)^2\right]^{-1/2}-\left[c+\left(x_1+\frac{R}{2}\right)^2\right]^{-1/2}-\left[c+\left(x_2-\frac{R}{2}\right)^2\right]^{-1/2}-\left[c+\left(x_2+\frac{R}{2}\right)^2\right]^{-1/2}+[c+(x_1-x_2)^2]^{-1/2}. \quad (3)$$

V_c is the Coulomb potential operator with x_1 and x_2 the coordinates of the two electrons and R is the internuclear distance. The external laser field interaction $V_{\rm ext}$ is of the form

$$V_{\rm ext}=\gamma I(t)^{1/2}(x_1+x_2)\cos(\omega t), \quad (4)$$

where ω and $I(t)$ are frequency (atomic unit) and intensity envelope (W/cm^2) of the external laser field. γ is a constant with value $0.533\,091\,78\times10^{-8}$ if $V_{\rm ext}$ is expressed in atomic units. We normally ramp the field so that after five cycles $E(t)$ or $I(t)^{1/2}$ attains its maximum E_0.

The wave function is obtained by iterating for the time step t to $t+\delta t$ the exponential operator solution with the time ordering operator $\hat{T}$,

$$\Psi(x_1,x_2,t+\delta t)=\hat{T}e^{-i[H(x_1,x_2,t)+V_{\rm ext}]\delta t}\Psi(x_1,x_2,t). \quad (5)$$

The exponential operator is evaluated directly using a split-operator technique [30] to give a unitary expression by separating the kinetic H_k and potential V_c operators,

$$\Psi(x_1,x_2,t+\delta t)=e^{-(i/2)\delta t H_k}e^{-i\delta t[V_c+V_{\rm ext}]}\times e^{-(i/2)\delta t H_k}\Psi(x_1,x_2,t)+O(\delta t^3). \quad (6)$$

The operation $\exp[-(i\delta t/2)H_k]\Psi(x_1,x_2,t)$ is performed by the spectral method which uses the fast fourier transform (FFT) technique [31]. The parameter c in V_c, the Coulomb potential, is taken as 1.0. Such a softened Coulomb potential removes the singularity and thus allows for efficient implementation of the exponential split-operator method [30]. Similar softened potentials have been used with success in N-body Coulomb problems [32], in quantum simulations of atoms [24,25], and in classical simulations of clusters in strong fields [28,29].

Calculations have been performed for various fixed internuclear distances R, with the laser field parallel to the molecular axis. The size of the grid used for the numerics is 256 a.u. with 1024 grid points in both x_1 and x_2 coordinates. An absorbing potential is used at the edge of the grid for both coordinates as in our original calculations on H_2^+ [22].

A. Energies and transition moments of 1D H_2

The ground state of H_2 is a singlet state, $X\,^1\Sigma_g^+$, the first excited state a triplet, $b\,^3\Sigma_u^+$, and the second singlet state is of ungerade symmetry, $B\,^1\Sigma_u^+$ [33]. The initial singlet ground state spatial wave function satisfies the symmetry property $\psi(x_1,x_2)=\psi(x_2,x_1)$ whereas the $b\,^3\Sigma_u^+$ has the symmetry $\psi(x_1,x_2)=-\psi(x_2,x_1)$. For the singlet B state one imposes in addition the antisymmetry $\psi(-x_1,-x_2)=-\psi(x_2,x_1)$. The exact electronic spatial function for each state is generated by propagating the field free equation (5) in imaginary time [34] by using initial Gaussian functions of the required symmetry. The exact initial wave functions are illustrated in Fig. 1 for each state at the internuclear distance $R=4$ a.u. The field free total energies are illustrated in Fig. 2. These were obtained by using the correlation function method after propagation in positive time [31] and then checked by evaluating $E=\langle\Psi|\hat{H}|\Psi\rangle$ with Ψ obtained from the imaginary time propagation method. In general three decimal digit accuracy was obtained in all cases. The 1D adiabatic potentials thus obtained are compared with the corresponding experimental values in Fig. 2. The 1D calculated surfaces are in good agreement with the experimental results, except that the 1D potentials are all shifted down, due to the fact that with $c=1$ in the softened Coulomb potentials, the ionization potential I_p of the H atom is 0.67 a.u. instead of 0.5 a.u., which is the 3D value. Choosing $c=1$ gives I_p of H_2^+ near the equilibrium, which is close to the 3D results. We do note that the true ground state equilibrium distance R is somewhat less than the 1D results; however, the 1D excited states agree generally well with the experimental values. In particular, the $B\rightarrow X$ transition energy is about the same in the 1D and 3D molecules for $R\geqslant 2$ a.u.

Of crucial importance in understanding CREI in H_2^+ is the divergent behavior of the $1\sigma_g\rightarrow 1\sigma_u$ electronic transition moment, i.e., $R/2$ [12,21], resulting in efficient coherent coupling of both states at high laser intensities and large R [16,17,22,23]. We illustrate therefore in Fig. 3 the $\mu=\langle X^1\Sigma_g^+|x_1+x_2|B^1\Sigma_u^+\rangle$ electronic transition moment obtained with the 1D initial electronic wave functions obtained as described above. Comparison with the highly accurate 3D *ab initio* calculations of Wolniewicz [35] shows excellent agreement between the 1D and 3D systems. Thus in both cases the H_2 $B\rightarrow X$ transition moment exhibits an initial $R/2$ rise as in H_2^+. However, due to electron correlation, the $B\rightarrow X$ transition moment has a maximum at $R\simeq 3$ a.u., with a value of 1.6, a minimum around $R=8$ a.u., and then the moment eventually reaches the $1s\rightarrow 2p$ atomic limit of 1.054 a.u. The 1D calculated moment reproduces quite satisfactorily the 3D results, thus confirming that the 1D model with $c=1$ in the Coulomb potential (3) can give quite reliable results for the electronic properties of H_2.

B. Ionization rates

The initial two-electron wave function corresponding to basically the $1\sigma_g^2$ configuration at $t=0$, $\Psi(x_1,x_2,0)$, is illustrated in Fig. 1(a). It corresponds to simple individual electrons localized at the deep wells of the total potential (3), i.e., $x_1=-R/2, x_2=+R/2$, or by symmetry $x_1=+R/2, x_2=-R/2$ (see Fig. 4). This initial function, obtained from propagating a Gaussian symmetric function in x_1,x_2 in imaginary time with the zero field Hamiltonian (2), (3) is then propagated in real time with the exact time-dependent Hamiltonian (1) as described above. The total ionization rate

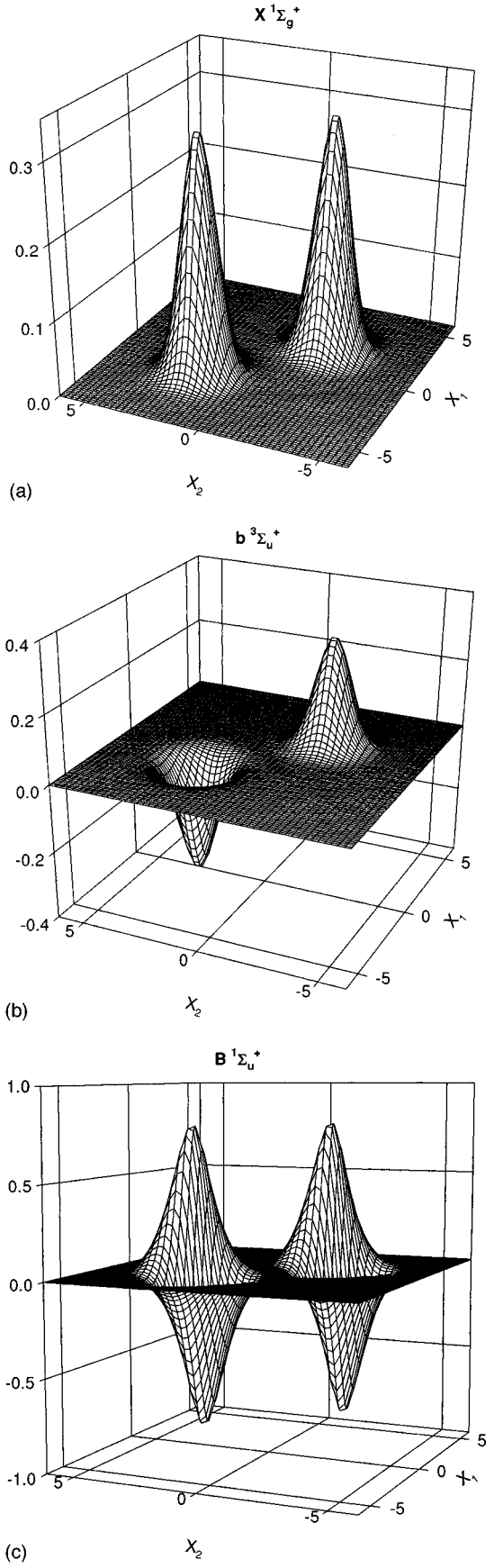

FIG. 1. Contour maps of 1D H_2 electronic wave functions: (a) the ground state $X^1\Sigma_g^+$, (b) the excited state with symmetry $b^3\Sigma_u^+$, (c) the excited state with symmetry $B^1\Sigma_u^+$.

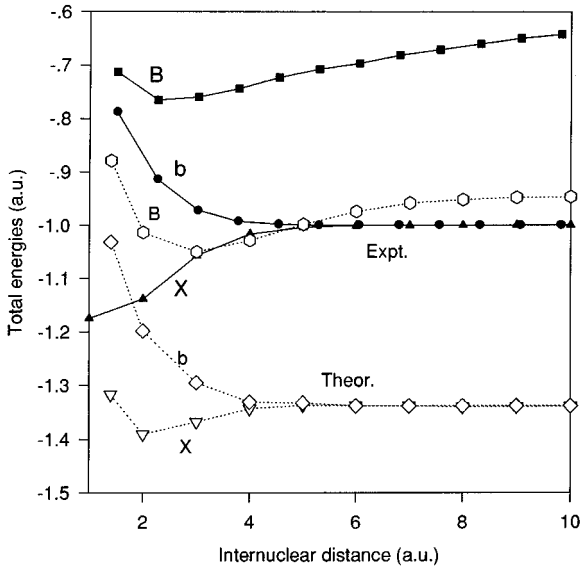

FIG. 2. Comparison of the calculated energies of the ground potential and the first two excited potentials with experimental ones: dotted lines — 1D calculations; solid lines — experiment.

$\Gamma(s^{-1})$ is therefore calculated from the logarithmic decrease of the total probability or norm $N(t)$,

$$\ln N(t) = -\Gamma t, \quad N(t) = \int |\Psi(x_1, x_2, t)|^2 dx_1 dx_2. \quad (7)$$

We illustrate in Figs. 5 and 6 ionization rates obtained by the above method for $\lambda = 1064$ and 532 nm as a function of the internuclear distance and various intensities . For comparison we include in Fig. 5(a) the 1D ionization rates of the single-electron molecular ion H_2^+ at $\lambda = 1064$ nm and $I = 10^{14}$ W/cm^2. Around equilibrium, ionization rates of H_2 are usually larger than those of H_2^+ molecular ions, as we obtained previously using 3D Cartesian finite element methods [36].

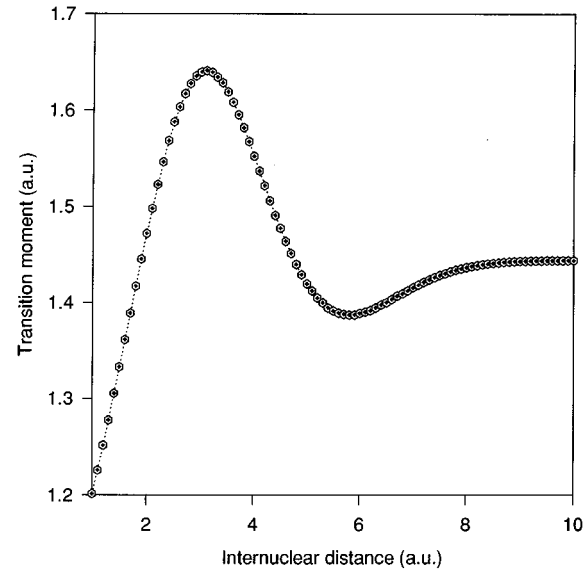

FIG. 3. 1D transition moments between the $X^1\Sigma_g^+$ and $B^1\Sigma_u^+$ states as a function of internuclear distance R.

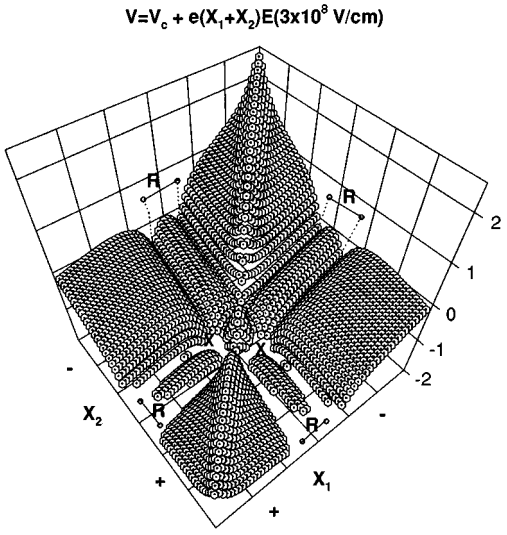

FIG. 4. Coulomb potential surface $V_c(x_1,x_2,R)$ [Eq. (4)] together with static laser interaction (5). $x_1(x_2)=R/2$ and $x_2(x_1)=-R/2$ correspond to the covalent resonance marked as X; $x_1=x_2=\pm R/2$ is the ionic resonance H^+H^- [33].

In the 1D case we have the results, e.g., at $R=2.0$ and 4.0 a.u., ionization rates are 1.2×10^{13},2.1×10^{13} and 2.2×10^{10},1.5×10^{11} s^{-1} for the H_2 molecule and H_2^+ molecular ion, respectively. However, at larger internuclear distance, e.g., $R=6$ a.u., the rates are reversed: 1.4×10^{13} s^{-1} for H_2 and 5.3×10^{13} s^{-1} for H_2^+. This is again evidence of CREI, i.e., in H_2^+, at large R, the $1\sigma_g-1\sigma_u$ energy separation decreases and the transition moment diverges as $R/2$. This creates unusual large radiative couplings between these two states. This effect is less important in H_2 where there is no degeneracy and no divergent moment (Figs. 2 and 3) as discussed next. The 1D H_2^+ results compare well with the more exact 3D calculations published previously for the same system and same excitation conditions [16,17]. Thus in both 1D and 3D H_2^+, extremely high ionization rates, exceeding that of the neutral H atom, are obtained between $R=7$ and 10 a.u. This was originally interpreted as due to a dynamic laser-induced localization thus leading to CREI [16]. Barrier suppression models [18–20] also predict such an enhanced ionization. Perusal of Figs. 5 and 6 shows maxima in the ionization rates of H_2 exceeding that of the separated neutral H atom by at least one order of magnitude. We turn next to discussion of this enhanced ionization phenomenon in H_2.

III. ENHANCED IONIZATION

Previous experiments [4] and calculations [9] on the multiphoton ionization of H_2 have emphasized the importance of charge resonance (CR) excitations in this two-electron system. Such excitations are mediated by divergent transition moments which are proportional to the internuclear distance R [12,21]. In the case of H_2^+, the first transition, $1\sigma_g\rightarrow1\sigma_u$, has in fact as stated before a divergent transition moment $\mu=R/2$ which leads to CREI, i.e., dynamic localization and static field barrier suppression from the laser pulse leads to large ionization rates of the single-electron molecular ion at critical large internuclear distance R_c, the

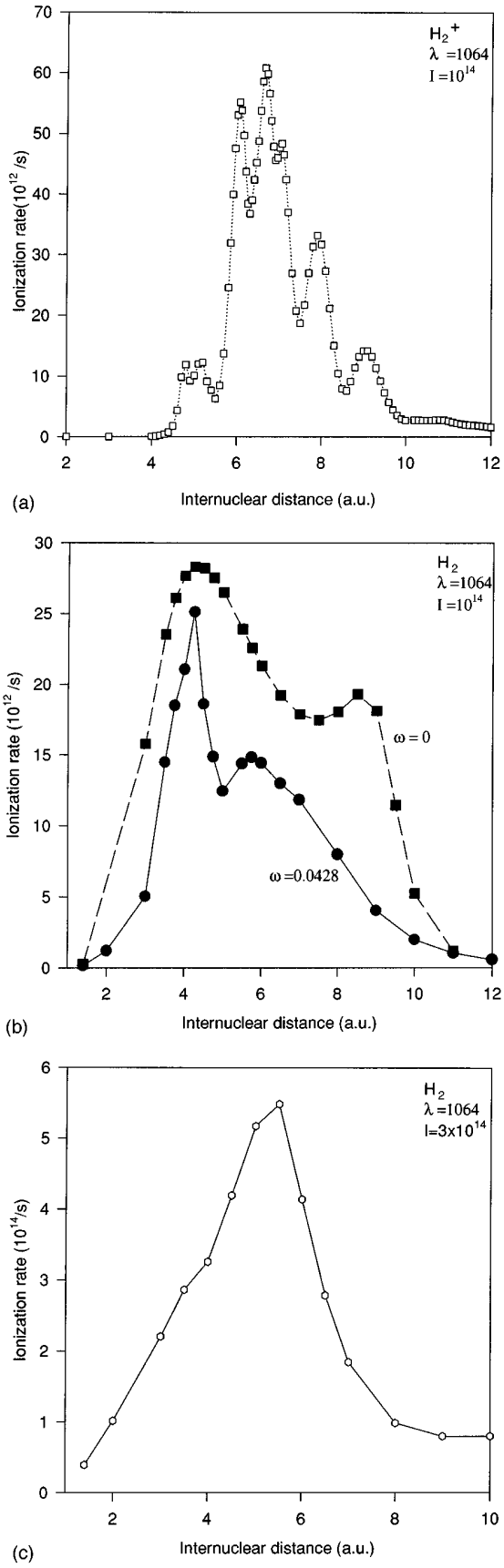

FIG. 5. 1D ionization rates at λ = 1064 nm as a function of R; (a) $-H_2^+$ ($I=10^{14}$ W/cm^2), (b) $-H_2$ ($I=10^{14}$ W/cm^2) (solid line — dynamic, ω = 0.0428; dots — static ω = 0), (c) $-H_2$ (3×10^{14} W/cm^2) .

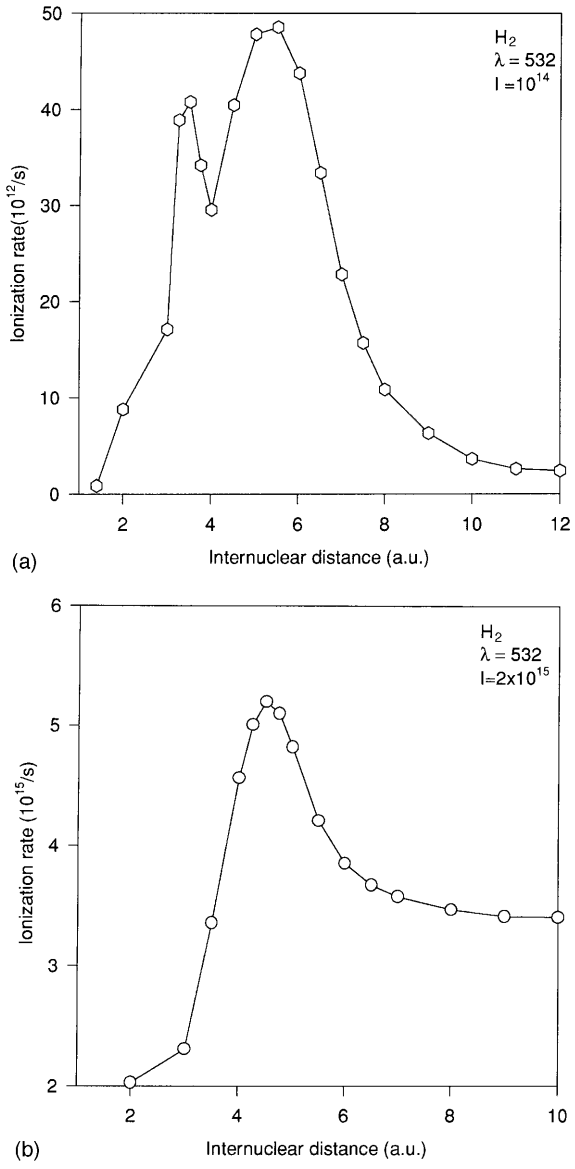

FIG. 6. Ionization rates for 1D H_2 at various R distances for $\lambda = 532$ nm: (a) $I=10^{14}$ W/cm^2, (b) $I=2\times10^{15}$ W/cm^2.

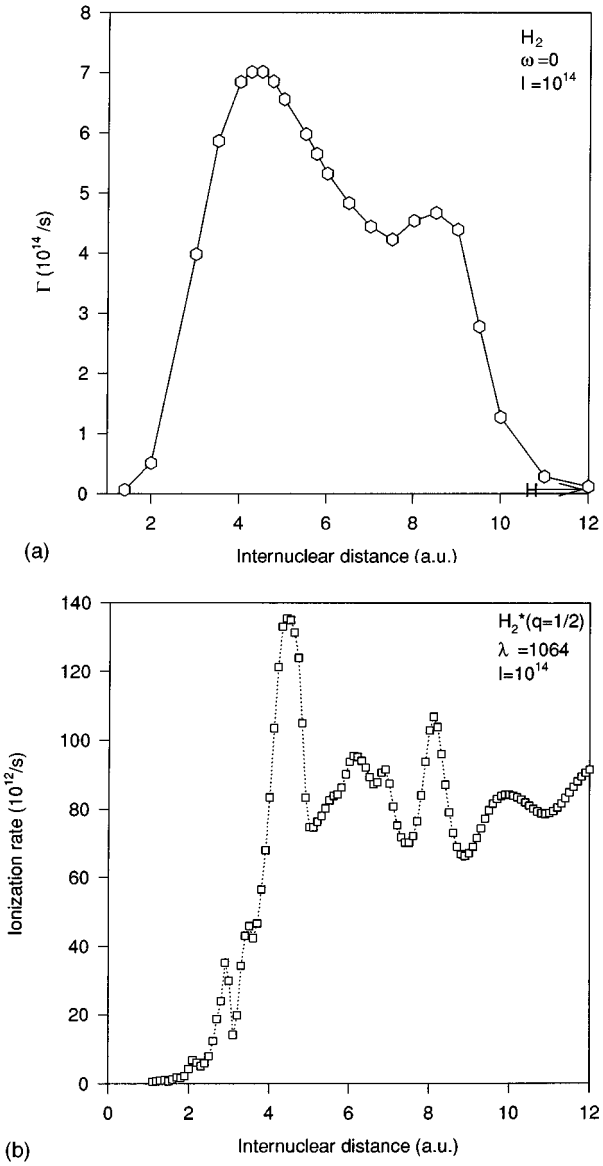

FIG. 7. (a) Linewidth Γ (s^{-1}) of the ground state of 1D H_2 as a function of internuclear distance R, in a dc field: $I=10^{14}$ W/cm^2, (b) ionization rates for 1D $H_2^*(q=1/2)$ as a function of internuclear distance R, $\lambda = 1064$ nm and $I=10^{14}$ W/cm^2.

rates of which are much larger than the atomic fragments. Perusal of Figs. 5 and 6 shows that the phenomenon of enhanced ionization persists in the two-electron system H_2.

The fundamental difference between H_2 and H_2^+ is that the ground state is non-degenerate at dissociation, i.e., at $R=\infty$, in the former whereas in the latter the degeneracy of the $1\sigma_g$,$1\sigma_u$ molecular orbitals at large R leads to the divergent transition moment. In H_2, the first transition moment from $X\rightarrow B$ (Fig. 3) behaves as $R/2$ up to $R\simeq3$ a.u. and continues on with the same values into the $B\rightarrow E,F$ transition [35]. Thus in Figs. 5(b) and 6(a), ionization maxima occur at $R\simeq4$ and 6 a.u., which can be correlated with the maxima of the transition moments of the $X\rightarrow B$ and $B\rightarrow E,F$ transition. (From Fig. 3, a maximum in the $X\rightarrow B$ moment at around $R\simeq6$ a.u. implies a change of configuration of the B state in that region, with another large moment appearing due to the $B\rightarrow E,F$ transition [35].) Thus at the lower intensity, 10^{14} W/cm^2, and for both wavelengths, 1064 and 532 nm, both enhanced ionization peaks seem to be correlated to these two CR transitions. At the higher intensities, 3×10^{14} and 2×10^{15} W/cm^2, Figs. 5(c) and 6(b), only one peak remains at $R\simeq4$ a.u.

It is now accepted that at high intensities and low frequencies, the static electric field at the peak of the pulse can lead to barrier suppression and rapid ionization of atoms [37,38] and molecules [13,18–20]. In order to test this idea in H_2 we have also plotted in Fig. 5(b) the dc ($\omega=0$) ionization rate of H_2 where one ramps a dc field for the same time as the $\lambda=1064$ nm pulse up to the constant field value for the intensity $I=10^{14}$ W/cm^2. One then calculates ionization rates and widths Γ of static field resonances as described previously [17]. The static field ionization rate or zero frequency ($\omega = 0$) [square line in Fig. 5(b)] is seen to exhibit two maxima, one at $R=4$ a.u. and the other at $R=8$ a.u. The static field resonance widths Γ (1 a.u. $= 4\times10^{16}$ s^{-1}) of the ground state, Fig. 7(a), are the same as the static ionization

rate, Fig. 5(b), which shows indeed that static field barrier suppression effects can produce enhanced ionization peaks at $R=4$ a.u. but also a further peak at $R=8$ a.u. (In fact the calculations show little excitation of the B state in H_2 as opposed to H_2^+.) The latter peak does not occur in any of the frequency-dependent laser excitation at $\lambda=1064$ nm (Fig. 5) and 532 nm (Fig. 6). The numerical results exhibited in Figs. 5–7 suggest therefore that as one goes to higher intensities, $I>10^{14}$ W/cm^2, only a single ionization peak remains important, i.e., at $R\simeq 4$ a.u. This differs from the single-electron result where two peaks usually occur at $R=7$ and 10 a.u. around 10^{14} W/cm^2 and merge at high intensities into one peak followed by a plateau at around $R\simeq 5$ a.u. [19,23].

One possible difference between H_2 and H_2^+ is the effect of electron screening. This is corroborated by our previous time-dependent Hartree-Fock and frozen core H_2 ionization rates where we found the frozen core results to be more reliable [36] and hence implying effective screening by the inner electron. Thus the first ionizing electron is not expected to be affected by two charges as in H_2^+ but rather a H_2^+ core with approximately $q=+1/2$ charge at each nucleus due to electron screening. The effect of such static screening is illustrated in Fig. 7(b), where we have calculated the ionization rate for the fictitious one-electron molecule $H_2^*(q=1/2)$, i.e., a neutral one-electron system in the presence of two $q=+1/2$ charge nuclei. This figure clearly shows two enhanced ionization peaks at $R=4$ and 8 a.u., akin to the static field case, Figs. 5(b) and 7(a). Electron screening clearly seems to play a role in the multiphoton ionization of H_2 at the shorter distance, $R=4$ a.u. The absence of visible enhanced ionization at $R=8$ a.u. in H_2 excludes therefore screening effects at large R. This can be rationalized by the fact that at the large R distances electron tunneling between the two nuclei, which creates the chemical bond, is suppressed by the laser field [16,17]. Similarly, electron correlation also localizes the electrons on each nucleus at large distances [33]. Excitation probabilities of the B state, which is expected to act as a doorway state [4,9], have been found to be under 10% and thus negligible in most of the cases studied here. This is in contrast to H_2^+, where excitation of the repulsive $1\sigma_u$ dominates the photophysics of the system as a result of efficient charge resonance excitation due to asymptotic degeneracy with the ground $1\sigma_g$ state and a divergent transition moment. Such is not the case in H_2, as explained in Sec. II A. Hence both laser field and electron correlation seem to combine to suppress enhanced ionization for $R>6$ a.u. in 1D H_2.

IV. ONE- AND TWO-ELECTRON IONIZATION

Contrary to the high frequency regime [26,27], lower frequency regimes such as $\omega=0.0428$ a.u. ($\lambda=1064$ nm) should show signatures of electron ionization via barrier suppression [17–20]. This is suggested by Fig. 4, where we show the total electrostatic potential, $V_c+V_{\rm ext}$, coming from V_c the Coulomb potential (3) and the static external potential at maximum field E, $V_{\rm ext}=-E(x_1+x_2)$. The dominant feature is the electron Coulomb repulsion ridge ($x_1=x_2$) on the symmetric diagonal which creates an impenetrable barrier. However, this ridge is lowered by the static part of the external field (at the maximum of the pulse). The second important feature is the one-electron nuclear Coulomb double wells for either coordinate x_1 or x_2, which is responsible for enhanced ionization (CREI), in single-electron diatomic ions such as H_2^+ [17–20]. The initial state wave function [Fig. 1(a)] is localized in the two separate deep wells on the antisymmetric diagonal $x_1=-x_2=\pm R/2$, corresponding to the covalent structure of H_2 (these are marked as x on Fig. 4). The ionic structure, H^+H^-, is situated on the Coulomb repulsion ridge at $x_1=x_2=\pm R/2$.

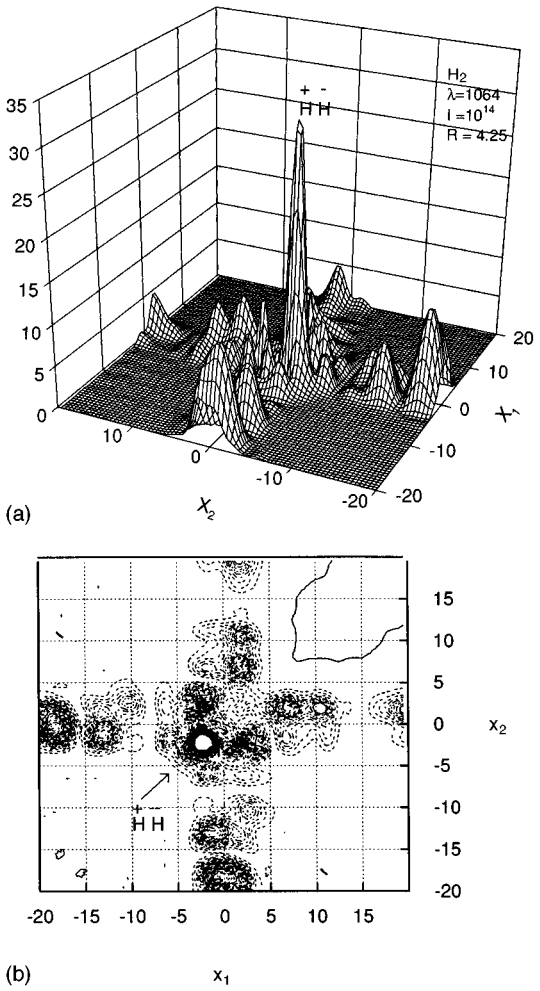

FIG. 8. Plot of the total density $|\psi(x_1,x_2,t)|^2$ after 20.75 cycles where $E(t)=E(\max)$ at $\lambda=1064$ nm, $I=10^{14}$ W/cm^2, $R=4.25$ a.u. [see Fig. 5(b)]. The major central peak corresponds to H^+H^-. (a) Vertical view, (b) horizontal view.

In the presence of the field, the simplest ionization path is for either electron to escape along the canals created by the bottom of either Coulomb well at $\pm R/2$ independently of the other. This can be seen in Fig. 8, where we show the electronic density $|\psi(x_1,x_2,t)|^2$ at $R=4.25$ a.u., the distance of maximum ionization at $\lambda=1064$ nm and $I=10^{14}$ W/cm^2 [see Fig. 5(b)]. The time t is 20.75 cycles so that the field has a maximum positive amplitude $E(\mathrm{V/cm})=5\times10^9[I(\mathrm{W/cm^2})/3.5\times10^{16}]^{1/2}$. In the present case $E(\max)=3\times10^8$ V/cm, so that the main electron flux occurs for negative x_1 and x_2. A major part of the electron density moves out independently along both canals of the nuclear Coulomb wells. Other notable features are clearly visible from Fig. 8(a). The

main wave packet of electron 1 (x_1 coordinate) as electron 2 propagates out is localized at $R=0$, in the middle of the double well. (For large R, e.g., at $R=6$, the second ionization maximum, this feature does not occur, i.e., the second electron wave packet is always localized in the right or left well). In fact examination of that part of the wavepacket remaining after the pulse has reversed sign [the $+x_1=+x_2$ quadrant in Fig. 8(a)] shows that when the field was negative, both electrons were localized in the lower well, $x_1=x_2=+R/2$. This reflects vestiges of the 1D static field barrier suppression effect in single-electron systems [17–20]. We conclude from Figs. 4 and 8 that both electrons can ionize independently by following the double well canals. This we can characterize as a *one-electron* process, as this appears as narrow wave packets of the second electron localized in one of the wells of the distorted remaining H_2^+. Figure 8(b) shows some wave packet remaining at $x_1=-x_2=\pm R/2$, corresponding to the initial covalent state H_2. But considerable density is trapped in the Coulomb ridge at $x_1=x_2=-R/2$. This is clear evidence of *laser-induced electron collision*, as this corresponds to the ionic structure H^+H^- discussed above. Figure 8 shows this effect to be important, as manifested by the dominant single peak in the middle of the figures.

Figure 8 suggests further a convenient method of separating one- and two-electron effects. At the lower intensity, $I=10^{14}$ W/cm^2, the ionizing electrons are propagating out in the narrow double canals due to the one-electron nuclear Coulomb double well, e.g., $V_c(|x_1|\leqslant\infty;|x_2|\leqslant R/2)$ and vice versa. This clearly corresponds to independent one-electron ionization as the second electron remains trapped in one of the remaining H_2^+ wells. However, as one goes to high intensities one expects the remaining H_2^+ electron to ionize by barrier suppression. This would mean, for example, that the narrow wave packets localized between $\pm R/2$ for either x_1 or x_2 would disperse *orthogonal* to the direction of the first ionizing electron, i.e., orthogonal to the canal directions, or equivalently by above barrier ionization in the 1D double wells (either x_1 or x_2).

In order to differentiate the one- and two-electron ionization process, we have therefore split our numerical grid box into four distinct regions: a, b, c, d (see left corner—Fig. 9). a is a box of dimension ± 16 a.u., containing initial H_2 which we also compare to a larger box d of dimention ± 32 a.u. The total box e has dimension ± 128 a.u. The four canals b have the width of a, 32 a.u., and allow us by integration to measure the total electron population ionizing independently along the electron nuclear Coulomb canals as discussed above. The remaining regions c should correspond therefore to a *two-electron* ionization process, since simultaneous large x_1 and x_2 coordinates indicate simultaneous two-electron ejection.

We show in Fig. 9 the various norms $N(t)$ of the two-electron population for the various regions defined above which are drawn in the left upper corner in Fig. 9. The results are shown for the maximum ionization rate $\Gamma_e=2.7\times10^{13}$ s^{-1} occurring at $R=4.25$ a.u. [Fig. 5(b)] for up to 20 cycles (75 fs) of the laser field. We note that the ionization rates Γ (s^{-1}) obtained from the logarithm of the norm [see Eq. (7)] are independent of box size (the total norms in regions a,d and the total box e are parallel). We see further

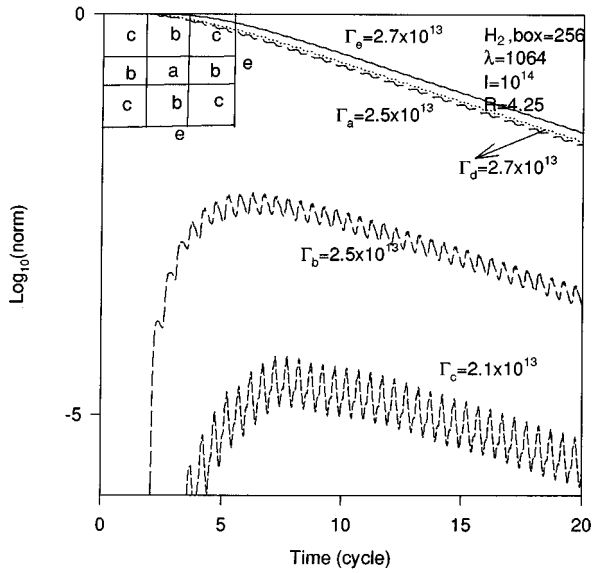

FIG. 9. Ionization rates $\Gamma(s^{-1})$ for regions defined in upper left corner: a: $|x|\leqslant 16$ a.u.; d: $|x|\leqslant 32$ a.u.; e: $|x|\leqslant 128$ a.u. $\lambda=1064$ nm, $I=10^{14}$ W/cm^2, $R=4.25$ a.u. (one cycle is equal to 3.55 fs).

that the direct two-electron processes Γ_c are at least two orders of magnitude less than the independent one-electron processes Γ_b at $I=10^{14}$ W/cm^2.

We turn next (Fig. 10) to the higher intensity, $I=3\times10^{14}$ W/cm^2 at $\lambda=1064$ nm and $R=4.25$ a.u., for which case we used a larger box of dimension $|x|\leqslant 256$ a.u. The norms in regions a ($|x|\leqslant$ 16 a.u.) and d ($|x|\leqslant$ 32 a.u.) are again parallel and these represent essentially the ionizing H_2 [Fig. 5(c)]. One notes steps in the norm curve at the end of each cycle where the field is essentially zero so that one infers the ionization occurs at the peaks of the field. Thus appreciable electron propagation occurs after the turn on of two cycles in the b canal regions. Thus just after two cycles,

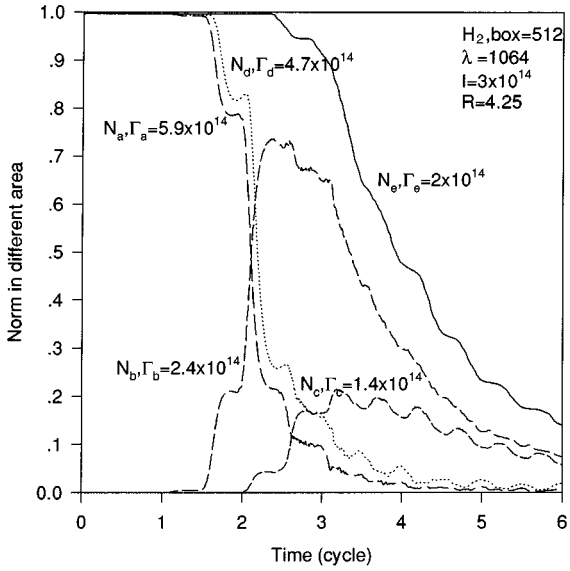

FIG. 10. Norm $N(t)$ in various regions a, b, c, d, e defined in Fig. 9. a: $|x|\leqslant 16$ a.u.; d: $|x|\leqslant 32$ a.u.; e: $|x|\leqslant 256$ a.u. $\lambda=1064$ nm, $I=3\times10^{14}$ W/cm^2, $R=R.25$ a.u. (one cycle is equal to 3.55 fs).

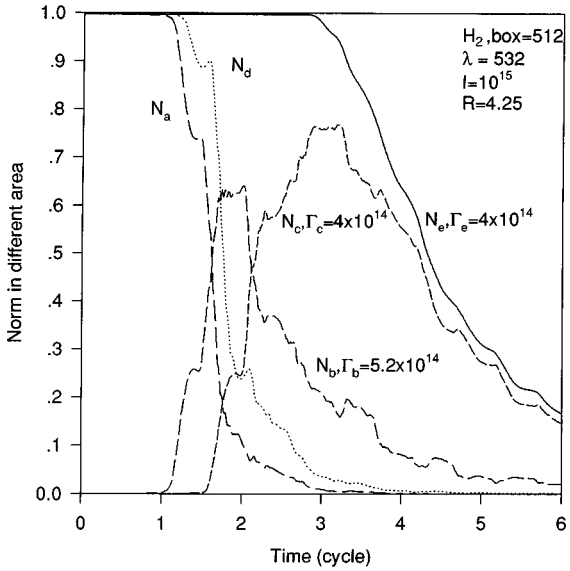

FIG. 11. Norm $N(t)$ in various regions a, b, c, d, e defined in Fig. 9. a: $|x| \leqslant 16$ a.u.; d: $|x| \leqslant 32$ a.u.; e: $|x| \leqslant 256$ a.u. $\lambda = 532$ nm, $I = 10^{15}$ W/cm^2, $R = 4.25$ a.u. (one cycle is equal to 1.8 fs).

70% of the electron population is in region b (N_b) with the remaining population in the box a (N_a) close to H_2. We reiterate that the canal region b corresponds essentially to $H_2{}^+ + e^-$. We note that the probability of one-electron processes as measured by N_b is at least one order of magnitude larger than that of two-electron processes as measured by the norm in region c, N_c.

Next we illustrate in Fig. 11 a calculation of H_2 at $\lambda = 532$ nm, $I = 10^{15}$ W/cm^2, $R = 4.25$ a.u. In spite of the two-cycle rise of the pulse, considerable electron population has now left the smaller boxes a and d surrounding the initial H_2: much of the population is transferred at 2 cycles in the independent electron propagation regions b, i.e., $H_2{}^+ + e^-$. After three cycles, most of the population is now to be found in the two-electron (large x_1, x_2) region c. Thus at around 3.5 cycles (6 fs), 75% of the electron population or norm $N(t)$ is to be found in the two-electron region c as measured by $N_c(t)$ and the remaining N_b is in the independent one-electron region b. Finally for larger times, the norm N_c of the function found in the two-electron region c is nearly identical to the total norm N_e for the total box of dimension 512 a.u. We infer from Fig. 11 that at $\lambda = 532$ nm and $I = 1 \times 10^{15}$ W/cm^2, direct two-electron photoionization dominates after three cycles of the laser pulse. The two-electron nature of the ionization is further confirmed by Fig. 12, where we plot the pair density $|\psi(x_1, x_2, t)|^2$ after 3.75 cycles (7 fs) when the field is maximum positive. Considerable density is found in the two quadrants $x_1 = -x_2$ (note no density is found in the region $x_1 = x_2$ due to the Coulomb repulsion), perpendicular to the Coulomb canals x_1 and $x_2 = \pm R/2$. We note that the two-electron ionization potential of H_2 goes from 51 eV at equilibrium ($R_e = 1.5$ a.u.) [39] to 27.2 eV asymptotically. Nevertheless, enhanced ionization is found to occur also around $R_c \simeq 4-5$ a.u. for intensities $I \geqslant 10^{15}$ W/cm^2 as a two-electron process.

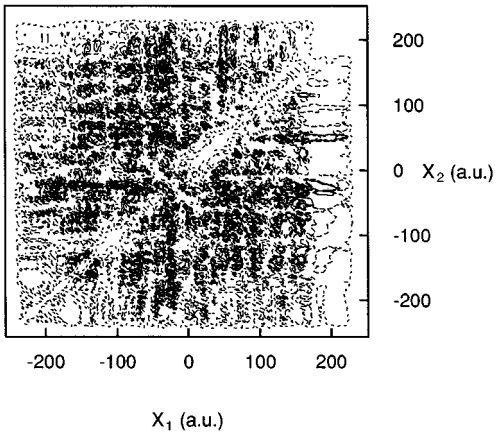

FIG. 12. Plane projection of $|\psi(x_1, x_2, t)|^2$ at 3.75 cycles for H_2 at $R = 4.25$ a.u., $\lambda = 532$ nm, $I = 10^{15}$ W/cm^2; box size is equal to 512 a.u.

V. CONCLUSION

We have used a 1D model of H_2 in order to calculate numerically from the TDSE (1) the ionization mechanism and rates at two wavelengths, $\lambda = 1064$ and 532 nm, for the two-electron molecule H_2 as a function of internuclear distance. The results illustrated in Figs. 5 and 6 show the propensity for this molecule to ionize preferentially at critical distances $4 \leqslant R_c \leqslant 6$ a.u. with rates exceeding that of the neutral H atoms by at least one order of magnitude. Such an effect, was shown previously to occur in one-electron symmetric diatomic ions and was called charge resonance enhanced ionization [17,19]. In the latter one-electron system, e.g., $H_2{}^+$, the charge resonance transition between molecular orbitals which are degenerate upon dissociation and which thus result in divergent transition moments, acts as the doorway transition for the photophysics of the one-electron system. In the case of H_2, the ground and first excited states are no longer degenerate (Fig. 2) so that the corresponding transition moment remains finite, Fig. 3, reaching asymptotically the atomic value. As a result the enhanced ionization region seems to be narrower than in one-electron active systems such as $H_2{}^+$. At high intensities ($I \geqslant 10^{15}$ W/cm^2), only one distance $R_c = 4-5$ a.u. becomes critical for the onset of enhanced ionization. This same critical value of ~ 5 a.u. at high intensities has been found for higher charged ions than $H_2{}^+$ and for polyatomics such as $H_3{}^{2+}$ [19,40]. Thus for the one-electron active system the high intensity enhanced ionization critical distance R_c seems to converge to 5 a.u., independent of charge. The same is found for two-electron systems. Since a barrier suppression model adequately explains this high intensity ($I \geqslant 10^{15}$ W/cm^2) R_c value in the case of one-electron active systems [19,20], we infer that the same mechanism, i.e., barrier suppression, applies also to multielectron systems.

Recent 1D and 3D classical calculations of two-electron systems such as H_2 and $He_2{}^{2+}$ also show low first ionization thresholds occurring at $R_c \simeq 4$ and 6 a.u. [28]. These classical results therefore agree with our quantum calculations. We suggest in Sec. IV that these are partly due to electron screening during the removal of the first electron, so that again a barrier suppression model applied to a single active

electron in the presence of a H_2^+ core [Fig. 7(b)] adequately reproduces the full quantum results.

At intensities $I \geq 10^{15}$ W/cm^2, for which $R_c \simeq 4-5$ a.u., our calculations indicate rapid simultaneous two-electron ejection. A detailed study of the two-electron wave function, Figs. 8–12, shows that at intensities below 10^{15} W/cm^2, especially around 10^{14} W/cm^2, one obtains independent electron ionization. Above 10^{15} W/cm^2, one finds essentially equal probability of finding both electrons at large distances, contrary to the lower intensity case. These results imply a threshold of about $\sim 10^{15}$ W/cm^2 for two-electron ionization in the visible frequency region.

ACKNOWLEDGMENTS

We thank Dr. S. Chelkowski (Sherbrooke) and Dr. P. B. Corkum (NRC-Ottawa) for useful discussions and the Natural Sciences and Engineering Research Council of Canada for support of the present research.

[1] J. R. Hiskes, Phys. Rev. **122**, 1207 (1961).
[2] G. R. Hanson, J. Chem. Phys. **62**, 1161 (1975).
[3] C. Cornaggia, D. Normand, J. Morellec, G. Mainfray, and C. Manus, Phys. Rev. A **34**, 207 (1986).
[4] J. W. J. Verschuur, L. D. Noordham, and H. B. van Linden Van den Heuvell, Phys. Rev. A **40**, 4383 (1989).
[5] P. H. Bucksbaum, A. Zavriyev, H. G. Muller, and D. W. Schumacher, Phys. Rev. Lett. **64**, 1883 (1990).
[6] A. Zavriyev, P. H. Bucksbaum, H. G. Muller, and D. W. Schumacher, Phys. Rev. A **42**, 5500 (1990).
[7] S. W. Allendorf and A. Szoke, Phys. Rev. A **44**, 518 (1991).
[8] H. P. Helm, M. J. Dyer, and H. Bissantz, Phys. Rev. Lett. **67**, 1234 (1991).
[9] A. D. Bandrauk, J. M. Gauthier, and E. Constant, J. Opt. Soc. Am. B **7**, 1422 (1990); J. Phys. (France) II **1**, 1033 (1991).
[10] A. D. Bandrauk and M. L. Sink, Chem. Phys. Lett. **57**, 569 (1978); J. Chem. Phys. **74**, 1110 (1981).
[11] E. E. Aubanel, J. M. Gauthier, and A. D. Bandrauk, Phys. Rev. A **48**, 2145 (1993).
[12] A. D. Bandrauk, *Molecules in Laser Fields* (Marcel Dekker, New York, 1993), Chap. 3.
[13] K. Codling and L. J. Frasinski, J. Phys. B **26**, 783 (1993).
[14] M. Schmidt, D. Normand, and C. Cornaggia, Phys. Rev. A **50**, 5037 (1994).
[15] E. Constant, H. Stapelfeldt, and P. B. Corkum, Phys. Rev. Lett. **76**, 4140 (1996).
[16] T. Zuo, S. Chelkowski, and A. D. Bandrauk, Phys. Rev. A **48**, 3837 (1993).
[17] T. Zuo and A. D. Bandrauk, Phys. Rev. A **52**, R2511 (1995).
[18] J. H. Posthumus, L. J. Frasinski, A. J. Giles, and K. Codling, J. Phys. B **28**, L349 (1995).
[19] S. Chelkowski and A. D. Bandrauk, J. Phys. B **28**, L723 (1995).
[20] T. Seideman, M. Ivanov, and P. B. Corkum, Phys. Rev. Lett. **75**, 2819 (1995).
[21] R. S. Mulliken, J. Chem. Phys. **7**, 20 (1939).
[22] S. Chelkowski , T. Zuo, O. Atabek, and A. D. Bandrauk, Phys. Rev. A **52**, 2977 (1995).
[23] S. Chelkowski, A. Conjustean, J. Zuo, and A. D. Bandrauk, Phys. Rev. A **54**, 3235 (1996).
[24] R. Grobe and J. H. Eberly, Phys. Rev. Lett. **68**, 290 (1992).
[25] S. L. Haan, R. Grobe, and J. H. Eberly, Phys. Rev. A **50**, 378 (1994).
[26] H. Wiedemann and J. Mostowski, Phys. Rev. A **49**, 2719 (1994).
[27] T. Zuo and A. D. Bandrauk, Phys. Rev. A **51**, R26 (1995).
[28] D. M. Villeneuve, M. Y. Ivanov, and P.B. Corkum, Phys. Rev. A **54**, 736 (1996).
[29] C. Rose-Petruck, K. J. Schafer, and C. P. J. Barty, SPIE Proc. **2523**, 271 (1995).
[30] A. D. Bandrauk and H. Shen, J. Chem. Phys. **99**, 1185 (1993).
[31] M. D. Feit, J. A. Fleck, and A. Steiger, J. Comput. Phys., **47** 412 (1982).
[32] *Multiple Time Scales*, edited by J. U. Brackhill, B. I. Cohen (Academic Press, Orlando, FL, 1985).
[33] J. C. Slater, *Quantum Theory of Molecules and Solids* (McGraw-Hill, New York, 1963), Vol. 1.
[34] K. C. Kulander, K. R. S. Devi, and S. E. Koonin, Phys. Rev. A **25**, 2968 (1982).
[35] L. Wolniewicz, J. Chem. Phys. **51**, 5002 (1969).
[36] H. Yu and A. D. Bandrauk, J. Chem. Phys. **102**, 1257 (1995).
[37] L. V. Keldysh, Sov. Phys. JETP **20**, 1307 (1965).
[38] P. B. Corkum, N. H. Burnnett, and F. Brunel, Phys. Rev. Lett. **62**, 1259 (1989).
[39] G. Dujardin, M. J. Besnard, L. Hellner, and Y. Malinovitch, Phys. Rev. A **35**, 5012 (1987).
[40] T. Zuo and A. D. Bandrauk, Phys. Rev. A (to be published).